Available online at www.sciencedirect.com
SCIENCE DIRECT
Diamond & Related Materials 14 (2005) 60–67
DIAMOND AND RELATED MATERIALS
www.elsevier.com/locate/diamond

Electro-deposition of adherent films of H_2-free quality diamond-like carbon materials on SS-304 substrates using nanocrystalline SnO_2 interlayer

M. Roy[a,*], A.K. Dua[a], A.K. Satpati[b]

[a]*Novel Materials and Structural Chemistry Division, Mod. Lab., Bhabha Atomic Research Centre, Room No. 2-203-H, Mumbai-400085, India*
[b]*Analytical Chemistry Division, Bhabha Atomic Research Centre, Mumbai-400085, India*

Received 17 November 2003; received in revised form 1 June 2004; accepted 30 June 2004
Available online 14 August 2004

Abstract

H_2-free diamond-like carbon (DLC) films are deposited on bare as well as nanocrystalline SnO_2-coated stainless steel (SS) 304 substrates. SnO_2 films are deposited by electrolysis of 10 mM $SnCl_2$ solution in nitric acid medium and then subsequently heating the sample in oxygen-ambient condition. The carbon films, on the other hand, are prepared by dissociative cleavage of methanol under high DC potential of 1 kV. Deposition conditions are optimised to get the best quality films, which are characterized by Raman spectroscopy, X-ray diffraction, X-ray photoelectron spectroscopy (XPS), and atomic force microscopy (AFM). It has been observed that films grown on SnO_2 interlayer are much more adherent when compared to those deposited on bare SS. Moreover, the quality of films on coated substrates is found to be much superior to those grown on bare SS. It is believed that the SnO_2 layer acts both as protective barrier against carbon diffusion into the SS substrate and also promotes nucleation due to anchorage of CH_3 and H^+ radicals (necessary for growth of DLC film) onto its oxygen deficient sites.

PACS: 81.15.Pq
Keywords: DLC; High sp^3 fraction; Electro-deposition; SnO_2 interlayer; Hydrogen-free

1. Introduction

Diamond-like carbon (DLC) films comprises of sp^2 and sp^3 bonded carbon atoms in varying proportions incorporated into an amorphous network and enjoy most of the exciting properties [1–3] exhibited by diamond. Hence, they find tremendous applications as protective coatings especially in the field of biomechanical engineering. One interesting application can be in the form of articulated human implants, wherein these implants (usually made of steel) are coated with either diamond or DLC films to make them biocompatible and corrosion resistant. DLC can address such biomedical problems often better than diamond because of their intrinsic smoothness and lower coefficient of friction. At the same time, they also offer better control over surface engineering. Moreover, DLC films are deposited at lower temperatures compared to diamond and thus are less prone to thermal stresses. Moreover, DLC coatings also promise a large number of industrial applications, e.g., storage tanks in chemical industries, etc., where large areas are required to be coated uniformly. DLC films are usually deposited by microwave plasma CVD [4], pulsed laser ablation [5] and arc discharge method [6]. However, the scalability to such a large extent and the cost effectiveness of these aforesaid techniques are still doubtful. Besides, it is also very difficult to get adequate nucleation of carbon on ferrous substrates, as carbon tends

* Corresponding author. Tel.: +91 22 25590292; fax: +91 22 5505151/5519613.
E-mail addresses: mainak73@apsara.barc.ernet.in, mainak73@yahoo.com (M. Roy).

0925-9635/$ - see front matter © 2004 Elsevier B.V. All rights reserved.
doi:10.1016/j.diamond.2004.06.040

to diffuse into them at high rates. Obviously, low-temperature deposition techniques are expected to give better results on such kind of substrates. Electro-deposition provides an easy and cheap way of depositing films even at room temperature uniformly over large areas and on intricate surfaces. Namba [7], Wang et al. [8] and Cao et al. [9] demonstrated the possibility of depositing DLC films from organic liquids using methanol as the electrolyte. Following the same route, we attempted room-temperature deposition of DLC on bare stainless steel (SS) substrates and found that the films so obtained are not at all adherent to SS and are more graphitic in nature. People have earlier reported that using single or multiple interlayers of metals (e.g., Cr, Ti, Co, Mo, etc.) [10–12] and/metal nitrides (e.g., TiN, CrN, etc.) [13,14] helped successful deposition of diamond and DLC on SS substrates. However, using high-melting oxide interlayers is not that common, as most of them (e.g., SiO_2) are known to delay the onset of carbon nucleation on them [15]. It is known from the literature that an adherent layer of nanocrystalline SnO_2 can be easily deposited on stainless steel substrates by electrochemical means, which led us to explore its feasibility as a barrier layer against carbon diffusion into the SS substrate. In this present article, we report room-temperature electro-deposition of quality diamond-like carbon films with very high sp^3/sp^2 ratio practically free from H_2 on stainless steel substrates using a nanocrystalline SnO_2 interlayer. The qualitative and the quantitative growth aspects of these films are also compared with those grown on bare SS. The plausible mechanism for deposition has been explored and the role of the intermediate layer discussed.

2. Experimental

2.1. Deposition of SnO_2 interlayer

The electrolyte consists of a 10 mM solution of tin dichloride (AR grade) prepared in 75 mM nitric acid (AR grade) medium. In order to obtain a stabilized solution, it is vigorously stirred for ~90 min at a bath temperature of ~80 °C. Electrolysis is carried out using a potentiostat AUTOLAB 100 (Eco Chemie make) in chronoamperometry mode using a conventional three-electrode cell configuration. A thoroughly cleaned stainless steel (SS-304) plate is used as the working electrode, and a tin metal plate separated by ~2 cm from it served as the counterelectrode. A saturated calomel electrode (SCE) is used as the reference. Films are deposited for ~160 min at a constant potential of −400 mV with effective current density varying from 1 to 10 mA/cm^2. HNO_3 medium partially oxidizes the metallic phase deposited to an oxide layer. Finally, the electrodeposited films are annealed at ~400 °C in oxygen-ambient condition for ~4 h. The optimised film thickness as estimated from steps in the films using a stylus is ~2.6 μm. Alternately, it is also estimated from the chronoamperometry plot using Faraday's laws of electro-deposition and has been found to agree well within the errors of the individual techniques. The films are characterized ex situ using XRD and Raman spectroscopy.

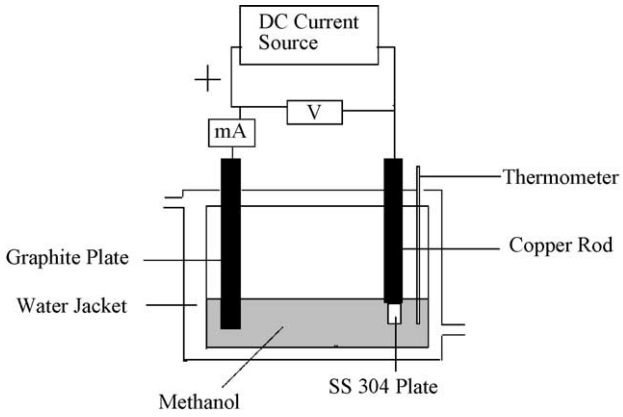

Fig. 1. Schematic diagram of the cell used for electro-deposition of DLC films.

2.2. Deposition of diamond-like carbon films

Schematic diagram for the deposition system is shown in Fig. 1. Analytically pure methanol is used as electrolyte. Bare as well as tin oxide-coated stainless steel (SS-304) plates are used as negative electrodes, while a graphite plate served as the positive electrode. The distance between the two electrodes is set to ~4 mm. The potential applied to the substrate is ~1 kV with respect to the positive electrode. The bath temperature is maintained at room temperature by constant water circulation. Typical deposition times are ~15–24 h. The DLC films have been characterized using X-ray diffraction, Raman spectroscopy, X-ray photoelectron spectroscopy (XPS) and atomic force microscopy (AFM).

XRD patterns are recorded in a Philips X-ray diffractometer PW 1710 using Cu Kα line from an X-ray generator operated at 30 kV and 20 mA. AFM studies are carried out under ambient conditions using a scanning probe microscope (SPM-Solver P47, NT-MDT, Russia) in contact mode using rectangular silicon nitride tips (tip radius ~10 nm). Raman spectra are recorded using LABRAM-1 spectrometer (ISA make) in a backscattering geometry and a spectral resolution of 2 cm^{-1}. The XPS spectra are recorded using Mg Kα radiation and constant pass energy of 13 eV.

3. Results and discussion

3.1. SnO_2 interlayer

Fig. 2 shows a typical chronoamperometry plot for the electro-deposition of tin oxide layer. The electrode current initially shoots up due to the leaching of the native chromium oxide layer present on the stainless steel substrate thereby exposing the metal and then gradually

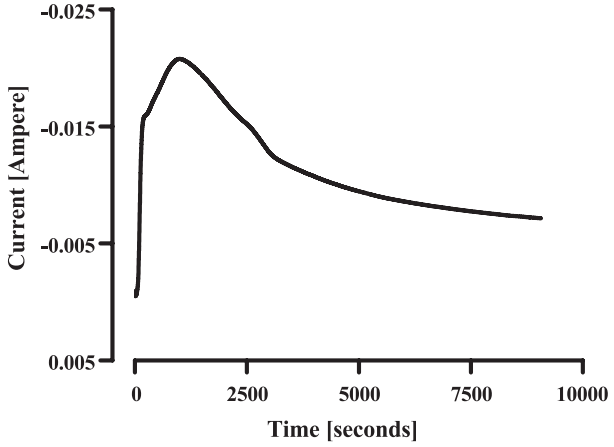

Fig. 2. Chronoamperometry plot of SnO_2 deposition on SS-304 substrates.

decreases with the formation of the tin oxide layer. A continuous coating is obtained within 15 min of deposition (as evidenced from the graph), which, upon annealing in oxygen-ambient conditions, transforms into an adherent semitransparent layer. The oxide layer prepared under the above-mentioned conditions reportedly exhibit nanocrystallinity [16]. Fig. 3a shows the XRD pattern of a typical SnO_2-coated stainless steel substrate. It exhibits very weak features at ~2θ=27°, 34° and 52°, respectively, corresponding to diffraction from the (110), (101) and (211) planes of the SnO_2 layer. The intense peaks at ~45° and 65° arise from the stainless steel substrate because the films are not sufficiently thick to block the signal from the SS substrate. Fig. 3b exhibits the micro-Raman spectra of the same sample. In contrast to a single-crystal SnO_2 or its polymicrocrystalline films which exhibit Raman bands at ~473(E_g), 632 ($A_{1\ g}$, the most intense band) and 773 ($B_{2\ g}$) cm^{-1} [17], our sample exhibits seven distinct features at ~225, 298, 355, 415, 556, 620 and 672 cm^{-1}, respectively. The intense peak at ~556 cm^{-1} and also the features at ~355 cm^{-1} are usually observed in the Raman spectra of nanometer-sized SnO_2 grains and has been interpreted to have arisen due to the dominating effects of the surface phonon modes over the bulk phonons in case of nanosized crystallites (typically less than 15 nm) [18,19]. The hump at ~620 cm^{-1} is possibly the down-shifted bulk phonon mode with $A_{1\ g}$ symmetry. Such variation of peak position can take place depending on the shape and state of aggregation of the SnO_2 particles together with the matrix in which they are embedded. In fact, a diffused peak at ~622 cm^{-1} has been reported for nanocrystalline SnO_2 [20] material present on the surface of ancient Chinese black mirrors. The peaks at ~670 cm^{-1} and ~300 cm^{-1} possibly corresponds to the Froehlich modes of SnO_2 nanoparticles observed due to the lowering of crystal symmetry and confinement-induced relaxation of selection rules (Δq=0). All these observations undoubtedly confirm that a layer of nanocrystalline SnO_2 has been formed on top of the stainless steel substrates.

3.2. Diamond-like carbon films

Upon high-voltage electro-dissociation of methanol, golden brown coloured films are deposited on SnO_2-coated SS substrates, while a blackish coat is obtained on bare SS. In order to evaluate adhesion properties of these films on SS, they are subjected to Scotch tape test. It is observed that the films grown on SnO_2-coated SS substrates are quite adherent, but those grown on bare SS are easily removed, exhibiting poor adhesion. This clearly indicates that SnO_2 interlayer promotes the growth of an adherent deposit on SS, otherwise difficult to achieve. Scratch test has also been performed qualitatively on the coatings, and the results support the aforesaid conclusions. During deposition, the electrode current density (ρ) is measured for various applied potentials, and their relationships are illustrated in Fig. 4a. It exhibits almost linear behaviour (solid lines to guide eyes) over the entire range, except for the deviations at high voltages (~1 kV). As expected, the current density for a given interelectrode distance is higher in the case of bare SS as compared to SnO_2-coated substrates. Fig. 4b shows the time dependence of the electrode current density at a fixed applied potential of 1000 V for films grown on both bare and SnO_2-coated substrates. Clearly, the current density decreases with deposition time. It is due to the formation of a continuous film (also confirmed from the absence of Ni and Cr peaks in XPS survey scans performed; to be

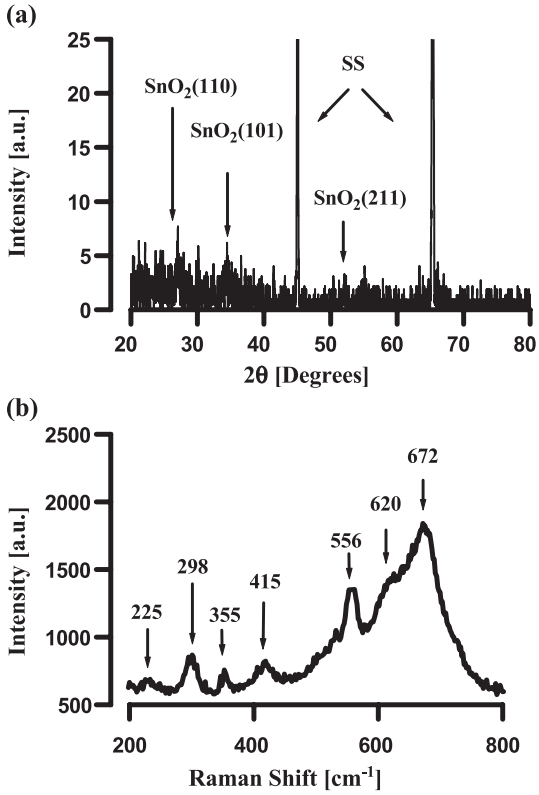

Fig. 3. (a) XRD pattern of the nanocrystalline SnO_2 interlayer. (b) Raman spectrum of the same SnO_2 interlayer.

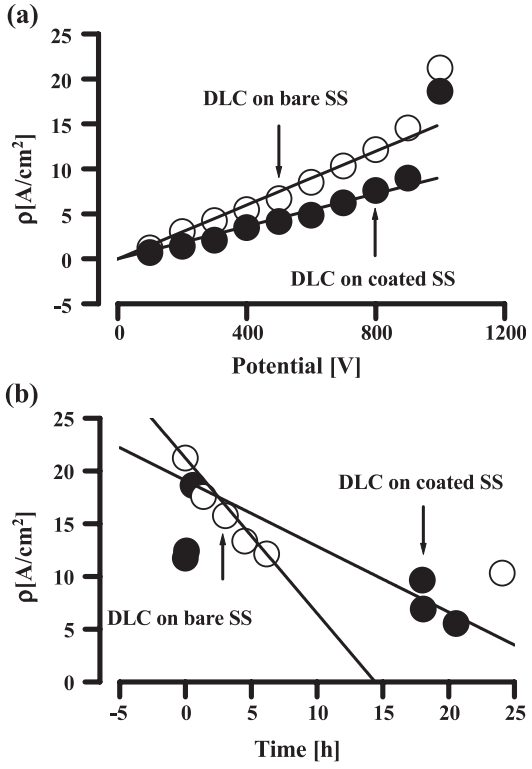

Fig. 4. (a) Plot of current density (ρ) vs. voltage at the start of DLC deposition (time 0 h). (b) Time-dependent plot of current density (ρ) at potential 1000 V.

discussed in details later on) of a highly resistive material (DLC?) that the electrode current starts dropping down steadily. Since this change in the electrode current density with time can only be attributed to the changing electrode resistance due to increased thickness of the deposited layer, a linear plot of current density vs. time is indicative of uniform deposition rates. Obviously, a steeper slope implies higher growth rate for samples grown on bare SS. The growth rate is estimated from film thickness (~5.17 μm for sample on bare SS and ~2.37 μm for that grown on coated substrate) and the time of deposition. The rate is found to be nearly double in case of films grown on bare SS (~3.6 nm/min) as compared to that grown on SnO_2-coated substrates (~1.9 nm/min). However, it should be borne in mind that the films are not adherent on bare SS, and it is quite impractical to compare their deposition rates. In fact, even on depositing for days together, hardly any adherent deposit is obtained on bare SS, which is quite expected due to the delayed nucleation of DLC on bare SS. Assuming that the electrode and cell resistance contribute in series towards the net effective resistance and from the known film thickness, the resistivity of the deposits is estimated to be ~10^8 Ω cm (~3.2×10^8 Ω cm for films on SnO_2-coated substrates and ~1.8×10^8 Ω cm for films on bare SS), typical for DLC films with very low bound hydrogen [21].

Fig. 5 shows the typical AFM topographies of films grown on bare SS and SnO_2 interlayer. It can be seen that the films grown on SnO_2-coated substrates are quite rough (RMS roughness ~150 nm) with average crystallite size ranging between 250 and 400 nm, while those grown on bare SS are relatively smooth (RMS roughness ~25 nm), and the particle size ranges between 100 and 250 nm. However, roughness of the SnO_2-coated samples depends very much on the roughness of the interlayer used, which, in turn, depends on the annealing temperature. XRD patterns (not shown here) of the deposits obtained on both bare and SnO_2-coated substrates clearly show that they are amorphous in nature. Fig. 6 shows the micro-Raman spectrum of the deposits obtained on bare and SnO_2-coated SS substrates, normalized to their respective time of acquisition. Clearly, both the spectra exhibit a broad band centred at ~1350 cm^{-1} assigned to the disorder-allowed zone edge mode of crystalline graphite (called the D-band) and a relatively sharp peak centred at ~1580 cm^{-1} corresponding to the optically allowed $E_{2\ g}$ zone centre mode of crystalline graphite (called the G-band), reportedly known to be the signatures for diamond-like carbon films. Since these Raman bands of diamond-like carbon are believed to monitor the state of sp^2-bonded material within the sp^3 matrix, an increased absolute intensity of the Raman spectrum for samples grown on bare SS is indicative of their higher sp^2 content. Besides, spectra of some samples (inset in the Fig. 6) also exhibit a broad band at ~600 cm^{-1} and a very weak feature at ~1075 cm^{-1}, which becomes discernable only on zooming. The band at ~600 cm^{-1} is reportedly [22] observed for unhydrogenated amorphous

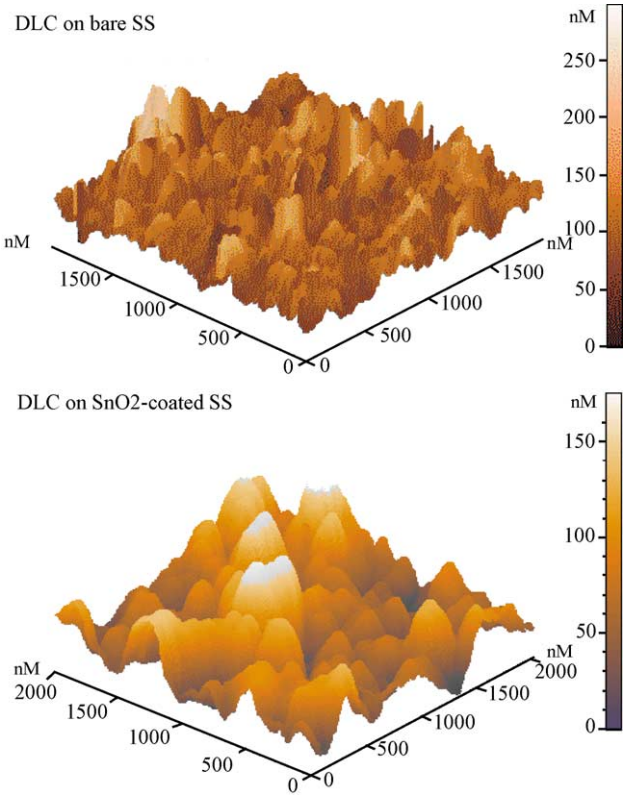

Fig. 5. Typical AFM topography of deposits on bare and SnO_2-coated SS substrates.

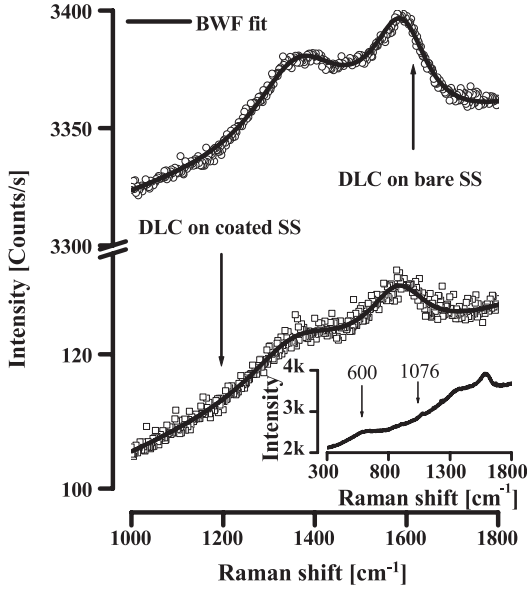

BWF fitted parameters

Substrates	ω_0	Q	Γ
Bare SS	1595.57	-7.08	142.77
Coated SS	1584.88	-15.82	152.11

Fig. 6. Micro-Raman spectra in the range 1000–1800 cm^{-1} of DLC films deposited on bare and SnO_2-coated SS-304 substrates. The spectra are fitted with BWF line shape, parameters tabulated below. Inset: a typical Raman spectrum in the spectral range 300–1800 cm^{-1} exhibiting a broad band at ~600 cm^{-1}.

carbon and roughly corresponds to the Raman inactive acoustic and out-of-plane optical vibrational modes of graphite [23,24]. However, it is not yet clear why such delocalised low-frequency modes become Raman active in hydrogen-free a-C and not in a-C:H. Tarmor et al. [22] tried to explain this phenomenon on the basis of matrix sensitivity of this Raman mode. Since the local bonding configurations around the sp^2 clusters are much more variable in a-C:H, the already broad low-frequency mode gets broadened further and also softer (hence, shifts towards the lower wave number) to such an extent that they are no longer apparent in the Raman spectrum of a-C:H. It is well known that the Raman cross-section in the visible range for the sp^2 sites is much higher than the sp^3 ones [25]. So, it is difficult to directly quantify the sp^3-bonding fraction present in DLC films using visible Raman spectroscopy. However, for hydrogen-free DLC films, Prawer et al. [27] proposed to fit the Raman spectrum using a Briet–Wigner–Fano (BWF) line shape after subtracting a linear background. The BWF line shape is described by

$$I(\omega) = \frac{I_0[1 + 2(\omega - \omega_0)/Q\Gamma]^2}{1 + [2(\omega - \omega_0)/\Gamma]^2} \quad (1)$$

where $I(\omega)$ is the intensity as a function of frequency (ω), I_0 is the maximum peak intensity, ω_0 and Γ are the peak position and full width at half maximum (FWHM), respectively, and Q is the BWF coupling coefficient. Following his proposition, we have fitted both the spectra in the range 1000–1800 cm^{-1} with a BWF line shape centred around the G-peak, a Lorentzian centred at ~1400 cm^{-1} for the D-band and a linear background to account for the luminescence. Though the origin of such Fano line shape of the Raman spectrum in DLC films is not properly understood as yet, the combination gives an excellent fit to the data as evidenced from χ^2 and R^2 values. The values of the fitted parameters thus obtained are tabulated at the bottom of the figure. It can be seen that the BWF line position (ω_0) moves down the energy and the coupling parameter (Q) decreases to a more negative value in case of films grown on coated substrates indicating an improvement of the quality of the deposit. From the empirical relationship between the Q parameter and sp^2 /sp^3 ratio [27], we estimate the sp^2 fraction in the bulk of the films grown on SnO_2-coated substrates to be less than 25% as compared to 35% in the case of films grown on bare SS. However, it should be borne in mind that these correlations were developed for carbon films deposited by entirely different techniques, and it may not strictly hold good for all types of carbons. Alternately, the Raman spectra may be fitted with either two Lorentzian or two Gaussian profiles, and from the different fitted parameters like band position, band width and intensity ratio I(D)/I(G), it is possible to get an idea about the different physical properties of DLC (e.g., optical band gap, hardness, etc.) and hence, the degree of sp^2 and sp^3 bonding in them. Figs. 7 and 8 shows the Raman spectra in

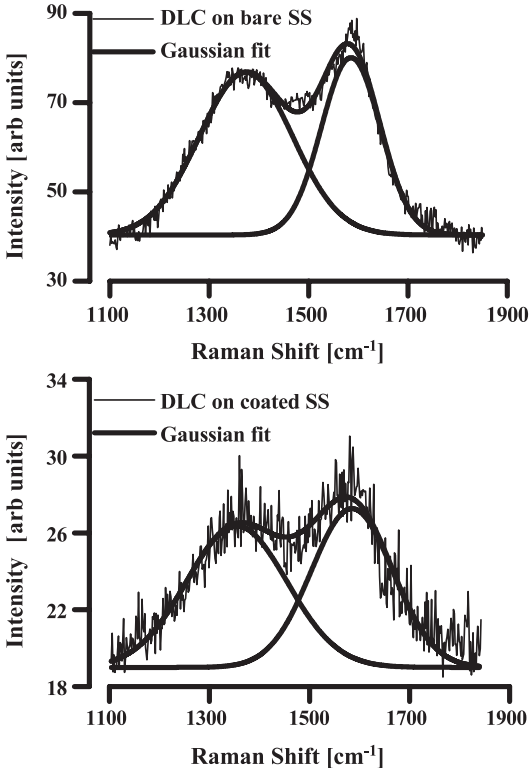

Fig. 7. Typical Raman spectra of DLC films on bare and SnO_2-coated SS substrates fitted with Gaussian line shape.

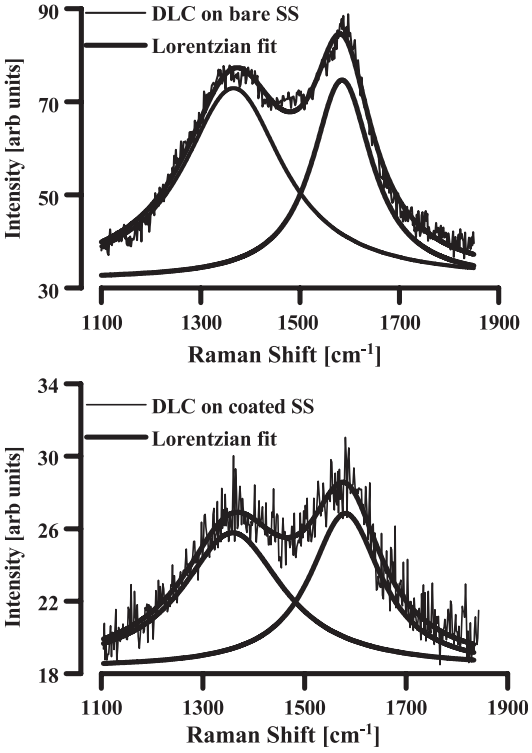

Fig. 8. Typical Raman spectra of DLC films on bare and SnO_2-coated SS substrates fitted with Lorentzian line shape.

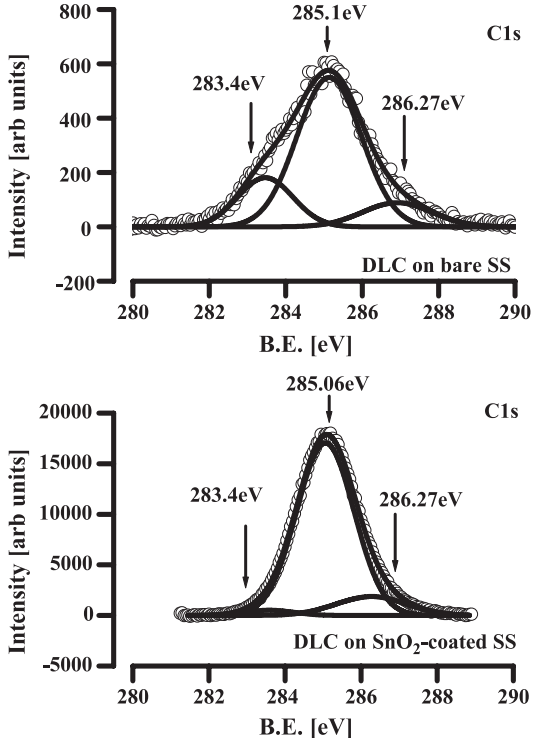

Fig. 9. Main core level C1s X-ray photoelectron spectra of diamond-like carbon films grown on bare and SnO_2-coated SS-304 substrates along with the deconvoluted features.

the wave number region 1100–1900 cm^{-1} for DLC films grown on bare and SnO_2-coated SS substrates fitted (after subtracting a linear background), respectively, with two Gaussian and two Lorentzian profiles. The results are shown in Table 1. Clearly, the trend observed for the Raman parameters using the two different line shapes are self-consistent. For samples grown on SnO_2-coated substrates, both the D and G bands broaden, shift to the lower wave number region (the shift is more pronounced in case of D band), and the $I(D)/I(G)$ ratio decreases significantly when compared to samples grown on bare SS. Though it is very difficult to make unambiguous conclusions from these trends due to contradicting reports in the literature, it is well accepted that the sp^2 content of DLC films increases with the $I(D)/I(G)$ ratio [28]. Obviously, optical band gap exhibits an opposite trend. Moreover, according to the model for amorphous carbon proposed by Beeman et al. [29], the downshift of the D and G bands of DLC films as observed in case of SnO_2-coated samples may be explained to be due to an increased bond angle disorder induced by the formation of sp^3-hybridized tetrahedral bonds. On the other hand, band broadening suggests that there is a decrease in the cluster size and increased stress in those carbon films. Following the works of Tarmor and Vassell [22] and Schwan et al. [26], who have extensively studied on the correlation of these Raman parameters with density, optical gap, hardness, hydrogen content and sp^2 /sp^3 ratio of the DLC films, the optical gap of our films can be roughly estimated to be ~1.5 eV and the hydrogen content to be negligibly small. The size of the sp^2 clusters embedded in the sp^3 matrix is estimated to be ~4 nm [26]. The sp^2 carbon fraction in the films has also been estimated from the G-band position [27], and that surprisingly shows very high values ~0.6 for samples grown on bare SS and ~0.5 for samples on coated substrates. Thus, in order to unambiguously confirm the sp^2 /sp^3 ratio of the DLC films, C1s XPS spectra is recorded in a slow scan mode. Fig. 9 shows the set of main core level C1s spectrum (along with deconvoluted features) of DLC films grown on SnO_2-coated and bare SS substrates. Typically, the spectra may be deconvoluted using

Table 1
Fitted Raman parameters of DLC grown on bare and coated SS

Substrates	Type of fitting	D band		G band		χ^2	R^2	$I(D)/I(G)$
		Position	Width	Position	Width			
Bare SS	Gaussian	1374.05	187.01	1585.19	118.00	4.34	0.98	1.44
	Lorentzian	1366.18	243.15	1584.68	144.03	4.45	0.98	1.61
SnO_2-coated SS	Gaussian	1354.52	200.56	1584.84	162.42	1.23	0.86	1.09
	Lorentzian	1358.71	239.52	1580.49	169.18	0.95	0.89	1.23

Gaussian into three distinct features at ~283.4, 285 and 287 eV. The feature at ~285 eV corresponds to the sp^3-hybridized carbon atoms, while that at ~283.5 eV corresponds to the sp^2-hybridized carbon atoms [30]. The third peak at ~287 eV may be associated with ester and/carboxyl groups [31] formed upon oxidation of the highly reactive surface components. The intensity ratio of the first two peaks gives an estimate of the sp^2/sp^3 carbon fraction. It is clearly evident from the deconvoluted features that the sp^2/sp^3 ratio is much more in case of samples on bare SS (~0.28) as compared to that on coated ones (~0.03). The sp^3-hybridized carbon atoms (as estimated from their respective peak areas) comprise about 86% of the total signal intensity in case of the SnO_2-coated samples as compared to only 68.7% in case of the bare samples, implying an improved DLC formation on the SnO_2 interlayer. These are very high values when compared to the results obtained from Raman analysis. Nevertheless, XPS provides information only about the surface layers and does not reflect the bulk property of the films, which can substantially differ from that of the surface layers. It is proposed that part of the sp^2 carbon sites on the surface gets converted to hydrogenated sp^3 sites under drastic conditions of deposition. XPS survey spectra of both the films have also been recorded with a view to cross-check their continuity. The essential feature of these spectra (not shown) is the absence of peaks corresponding to nickel and other components of stainless steel substrates, further confirming complete coverage of the substrate area. Based on these above results, a mechanism has been proposed for the deposition of DLC films via dissociative cleavage of methanol. CH_3OH gets polarised and transported with the electrolyte under high electric field as

$$2CH_3OH + 2H_2O \rightarrow 2CH_3^+ + 2H^+ + 4OH^- \quad (1)$$

$$2H^+ + 2e^- \rightarrow H_2 \uparrow \quad (2)$$

$$2CH_3^+ + 2e^- \rightarrow 2CH_3 \cdot \quad (3)$$

Thus, the cathode surface would experience the presence of very high concentration of methyl radicals and H^+ required for the deposition of DLC films. The nanocrystalline SnO_2 interlayer with very high surface/volume ratio and large number of oxygen-deficient sites provides anchorage to these $CH_3\cdot$ radicals along with H^+, thereby facilitating the bond breaking and bond making of the sp^2 and sp^3 bonded carbon atoms at the film surface, thereby promoting the growth of DLC films. Moreover, it also serves as a barrier against carbon diffusion into the SS substrates and thus helps in accelerating the onset of nucleation. A direct evidence of SnO_2 acting as a barrier layer comes from the bulk carbon analysis of the samples. The carbon films are first removed by grinding; then the samples are analyzed chemically using combustion technique where from carbon flux, i.e., the weight of carbon diffusing into the bulk of SS substrates per unit area per unit time is estimated. The results of chemical analysis are shown in Table 2. As expected, the diffused carbon flux is ~3.9 times more in case of bare SS as compared to that of the coated substrates, thereby confirming our conclusion that SnO_2 acts as a barrier against carbon diffusion into the SS substrates.

4. Conclusions

It has been demonstrated that in contrast to bare SS on which DLC films are not adherent at all, fairly adherent films of diamond-like carbon materials can be deposited electrochemically even at room temperature on SnO_2-coated SS substrates using CH_3OH as the electrolyte. The films have been extensively characterised using Raman spectroscopy, XPS and AFM. Though the films deposited on coated substrates are found to be rough, they are of much superior quality from sp^2/sp^3 ratio point of view. The sp^2/sp^3 ratio has been estimated both from Raman spectrum analysis and XPS and is found to be fairly low (~35–25%), lower in case of the SnO_2-coated samples. The films are also found to be practically free from hydrogen. The nanocrystalline SnO_2 interlayer has been shown to act both as protective barrier against carbon diffusion into the SS substrates and promote nucleation due to anchorage of CH_3 and H^+ radicals (necessary for growth of DLC film) onto its oxygen-deficient sites, thereby accelerating the growth of DLC films.

Acknowledgement

The authors are thankful to Mr. Jagannath, TP&PE Division, BARC for recording XPS and Mrs. Shilpa Sawant, NM&SC Division, BARC for recording the AFM images. The authors are thankful to Mr. Kunal Mali,

Table 2
Bulk carbon analysis of samples

Samples	Weight (g) (without DLC film)	Bulk carbon (%)	Deposition		Diffused carbon flux[a]
			Area (cm^2)	Time (s)	($g\ cm^{-2}\ s^{-1}$)
Ref. SS substrate	0.9282	0.0427	–	–	–
DLC on bare SS	1.1123	0.0748	1.65	86760	2.49×10^{-9}
DLC on SnO_2 layer	1.1102	0.0489	1.45	74412	6.38×10^{-10}

[a] Diffused carbon flux={(% Bulk $carbon_{Sample-Reference}$)×Weight/100}/(Area×Time).

NM&SC Division, BARC for his kind cooperation in the work. The authors also thank Dr. S.K. Kulshreshtha, Head NM&SC Division, BARC and Dr. T. Mukherjee, Associate Director Chemistry group, BARC for their keen interest in the work.

References

[1] H. Kakiuchi, T. Kobayashi, T. Terai, Nucl. Instrum. Methods Phys. Res., B Beam Interact. Mater. Atoms. 166–167 (2000) 415.
[2] K.J. Clay, S.P. Speakman, N.A. Morrison, N. Tomozeiu, W.I. Milne, A. Kapoor, Diamond Relat. Mater. 7 (1998) 1100.
[3] R. lappalainen, H. Heinonen, A. Anttila, S. Santavirta, Diamond Relat. Mater. 7 (1998) 482.
[4] Elzbieta Staryga, Chaos, Solitons Fractals 10 (1999) 2075.
[5] A.K. Sharma, R.J. Narayan, J. Narayan, K. Jagannadham, Mater. Sci. Eng., B, Solid-State Mater. Adv. Technol. 77 (2000) 139.
[6] A.V. Stanishevsky, L. Yu. Khriachtchev, R. Lappalainen, M. Rasanen, Diamond Relat. Mater. 6 (1997) 1026.
[7] Y. Namba, J. Vac. Sci. Technol., A 10 (1992) 3368.
[8] H. Wang, M. Shen, Z. Ning, C. Ye, C. Cao, H. Dang, H. Zhu, Appl. Phys. Lett. 69 (1996) 1076.
[9] C. Cao, H. Zhu, H. Wang, Thin Solid Films 368 (2000) 203.
[10] A.K. Sikder, T. Sharda, D.S. Misra, D. Chandrasekaram, P. Selvam, Diamond Relat. Mater. 7 (1998) 1010.
[11] A.K. Sikder, T. Sharda, D.S. Misra, D. Chandrasekaram, P. Veluchamy, H. Minoura, P. Selvam, J. Mater. Res 14 (3) (1999) 1148.
[12] Q.H. Fan, J. Gracio, E. Pereira, N. Ali, W. Ahmed, J. Mater. Res 15 (11) (2000) 2330.
[13] G. Negrea, G. Vermesan, J. Optoelectron. Adv. Mater. 2 (5) (2000) 698.
[14] W.P. Hsieh, D.Y. Wang, F.S. Shieu, J. Vac. Sci. Technol., A 17 (1999) 1053.
[15] N.A. Fox, M.J. Youh, W.N. Wang, J.W. Steeds, H.-F. Cheng, I.-N. Lin, Diamond Relat. Mater. 9 (2000) 1263.
[16] S.T. Chang, I.C. Leu, M.H. Hon, Electrochem. Solid-State Lett. 5 (8) (2002) C71–C74.
[17] A. Dieguez, A. Romano-Rodriguez, J.R. Morante, U. Weimar, M. Schweizer-Berberich, W. Gopel, Sens. Actuators, B, Chem 31 (1996) 1.
[18] P.S. Peercy, B. Morosin, Phys. Rev., B 7 (1973) 2779.
[19] J. Zuo, C. Xu, X. Liu, C. Wang, J. Appl. Phys. 75 (1994) 1835.
[20] C. Wang, B. Lu, J. Zuo, S. Zhang, S. Tan, M. Suzuki, W.T. Chase, Nanostruct. Mater. 5 (4) (1995) 489.
[21] A. Grill, V. Patel, S. Cohen, Diamond Relat. Mater. 3 (1994) 281.
[22] M.A. Tarmor, W.C. Vassell, J. Appl. Phys. 76 (6) (1994) 3823.
[23] R. Al-Jishi, G. Dresselhaus, Phys. Rev., B 26 (1982) 4514.
[24] C. Oshima, T. Aizawa, R. Souda, Y. Ishizawa, Y. Sumiyoshi, Solid State Commun. 65 (1988) 1601.
[25] N. Wada, P.J. Gaczi, S.A. Solin, J. Non-Cryst. Solids 35 (1980) 543.
[26] J. Schwan, S. Ulrich, V. Batori, H. Ehrhardt, S.R.P. Silva, J. Appl. Phys. 80 (1) (1996) 440.
[27] S. Prawer, K.W. Nugent, Y. Lifshitz, G.D. Lempert, E. Grossman, J. Kulik, I. Avigal, R. Kalish, Diamond Relat. Mater. 5 (1996) 433.
[28] B.K. Tay, X. Shi, H.S. Tan, H.S. Yang, Z. Sun, Surf. Coat. Technol. 105 (1998) 155.
[29] D. Beeman, J. Silverman, R. Lynds, M.R. Anderson, Phys. Rev., B 30 (1984) 870.
[30] J.C. Lascovich, R. Giorgi, S. Scaglione, Appl. Surf. Sci. 47 (1991) 17.
[31] I. Kulak, A.I. Kokorin, D. Meissner, V.G. Ralchenko, I.I. Vlasov, A.V. Kondratyuk, T.I. Kulak, Electrochemistry Communication 5 (2003) 301.